Hindawi
Advances in Civil Engineering
Volume 2022, Article ID 9292794, 12 pages
https://doi.org/10.1155/2022/9292794

Research Article

A Simple Benchmark to Evaluate the Influence Parameters of the Microstructure of the Masonry Wall on Capillary Water Migration Dynamic

Martial Nde Ngnihamye,[1] **Fabien Kenmogne**,[1] **André Abanda**,[1,2] **Michel Mbessa**,[3] **Jean-De-La-Croix Gnappoun**,[1] **and Didier Fokwa**[1]

[1]*Department of Civil Engineering, Advanced Teacher Training College of the Technical Education, University of Douala, Douala, Cameroon*
[2]*Department of Civil Engineering, National Advanced Polytechnical School of Douala, University of Douala, Douala, Cameroon*
[3]*Department of Civil Engineering, National Advanced School of Public Work of Yaoundé, The University of Yaoundé 1, Yaoundé, Cameroon*

Correspondence should be addressed to Martial Nde Ngnihamye; martialnde@yahoo.fr

Received 29 July 2022; Accepted 21 September 2022; Published 3 October 2022

Academic Editor: Chao Dou

The effects of masonry wall parameters on the water's migration are deeply explored via the experimental laboratory simulation method. At this end, an experimental device consisting of a water tank in which a masonry block wall has a contact of around one centimeter with the water at its base is designed. The variation of the compactness of masonry blocks is obtained by compacting the concrete blocks with a hydraulic block press. The investigations consist of the monitoring of moisture front and moisture rate as a function of porosity, obtained by varying the compactness of the masonry wall, and the granular class of sand constituting the masonry. The determination of the granular sand classes was made from the NF P 18-101 standard. Three granular classes of sand were obtained using sand from the Logbadjeck quarry: 0/0.315 mm, 0.63/1.25 mm, and 2.5/5 mm. The obtained results show that the device is a good tool for the experimental analysis of the behavior of different masonry walls under water migration, which are in agreement with existing models in the literature.

1. Introduction

Masonry is a construction system that has been widely used since the beginning of civilization and is still used throughout the world [1]. Building materials and those cementatious are the most used for the construction of structures. These materials are usually consisting of aggregates, cement, and water. Water is the key ingredient, which when mixed with cement, forms a paste that binds the aggregate together, and during the hydration process, the consistency of the material gradually changes from fluid to firm and then reaches the hardening of concrete.

During the hydration process, several microstructural phenomena appear, leading to the creation of two forms of porosities. The ITZ around the aggregates, where the presence of aggregates belongs to a determined granular class, disturbs the normal evolution of the hydrates, leading to an increase in the porosity in this zone. The compaction by vibration or other means, of the cementatious materials during their implementation, modifies the microporous structure of the material but does not make it impermeable to the migration of moisture.

It had been proved that the cementatious materials used in construction are essentially porous [2–5]. This is why they are subjected to almost permanent exchanges with their external environment, thus posing the durability problem of structures [6–9]. In fact, apart from the deterioration of the living comfort and health of the occupants, the migration of

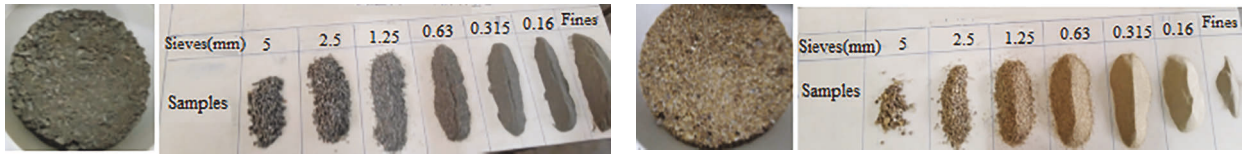

(a) (b)

Figure 1: Texture and visual appearance of sand samples (a) LQS and (b) MQS.

moisture in the microstructure of these materials, sometimes accompanied by the transport of aggressive agents, endangers the durability of the structure. Moreover, the increase in the moisture content can negatively impact the building's heating process, leading to an increase in the power consumed during heating [10]. For these obvious reasons, it seems necessary to have a deepened knowledge of the hygrometric behavior of cementatious materials. Most works on this subject aim to highlight the extreme complexity of the dynamics of moisture migration in these cementatious materials, which present a highly microporous and very complex multiphase structure. This induces particular characteristics such as capillary absorption and hygroscopicity. This is why some authors conducted channeled reflections, focused on the role of the material's microstructure in the dynamics of humidity migration [11, 12], and experimental tools have been developed [13–15], as well as mathematical models [16, 17].

The aim of this work is to investigate experimentally the dynamics of moisture migration in masonry walls. To this end, a metrology will be developed which will allow the describing of the dynamic of moisture migration in an instrumented wall. Then, after having characterized the microstructure of the concrete blocks (porosity of ordinary and compacted concrete blocks, porosity in relation to the granular class of sand used for the manufacture of concrete blocks), the influence of the compactness will be first analyzed, following at the end by the analysis of the influence of a granular class of sand used for the manufacture of concrete blocks.

2. Materials

2.1. Origin of Raw Materials. The cement used to make the breeze blocks comes from the manufacturer Dangoté, whose production plant is located in the Douala IV subdivision. It is a compound Portland cement (CEM II 32.5), manufactured according to the NF EN 197 − 1 standard, sold in 50 kg bags, and with a strength class of 32.5 N/mm^2. The mixing water necessary for the hydration of the cement comes from the Cameroon water utility corporation. Two types of sand are used independently, the Logbajeck quarry sand (LQS) (see Figure 1(a)) and the Moungo quarry sand (see Figure 1(b)). The LQS is used to highlight the influence of the granular classes. This sand is mainly composed of metamorphic rocks (gneiss) made up of quartz, mica, and feldspar, extracted from the Logbajeck quarry located about 50 km from Douala. The MQS is used to highlight the influence of the compactness of the breeze blocks. This sand comes from a deposit whose parent rock is magmatic, of volcanic type (high concentration of quartz). This sand is extracted from the Moungo river bed by dredging with pumps, or in an artisanal manner using shovels and dugout canoes.

2.2. Characterization of Raw Materials. The granulometric analysis of sand samples according to the NF EN 933-1 standard is carried out using an oven, a 0.01 g precision balance, and standardized sieves (Figures 2(a)–2(c)). The determination of the granular classes of sand is then carried out from the NF P 18 − 101 standard. These granular classes will be used to simulate in the laboratory their influence on the dynamics of moisture migration in the masonry wall.

For the calculation of exact masses of sand necessary for the manufacture of the breeze blocks, the determination of the apparent densities of sands was carried out according to the prescriptions of the NF P 18-554 standard. Thus, after weighing the respective masses of the empty container M_1 and the container filled with the sand sample M_2, and after measuring the volume V of the container, the apparent densities of the samples are determined by the following equation:

$$\rho = \frac{(M_2 - M_1)}{V}. \quad (1)$$

2.3. Composite Formulation and Manufacturing. The proportions of the mortar components taken into account in this experiment are those recommended by the manufacturer of the binder used (Dangoté Cement CPJ 32.5). The W/C ratio is kept constant and equal to 0.5 for all manufactured mortars. The sand dosages, cement, and water per 110 liters of mortar are given in Table 1. After mixing the different components, $15 \times 20 \times 40\,cm^3$ and $20 \times 20 \times 40\,cm^3$ breeze blocks are produced manually (ordinary breeze blocks) and with the help of a breeze block press (vibrated breeze blocks) (Figure 3(a)). The block press used allows a pressure of about 5 kg/mm^3 to be applied. The breeze blocks are then cured for 72 hours, according to the requirements of the NF EN 13670 standard, to ensure complete hydration of the cement. The cure is followed by a drying period in ambient air, approximately 29^oC for 168 hours.

(a) (b) (c)

Figure 2: (a) Standardized sieves, (b) 0.01 g precision balance, (c) Oven.

Table 1: Dosage of sand, cement and water necessary to have 110 liters of mortar.

Constituents	Units	Dosages
Cement	Kilogram (kg)	50
Sand	Liter (l)	110
Water	Liter (l)	25

2.4. Characterization of Composites. Cubic mortar blocks of dimensions $4 \times 4 \times 4\,cm^3$ were made for the determination of the porosity of each simulated wall type (Figure 3(b)). A device for measuring the percolating porosity (n) of the blocs has been manufactured following the principle diagram of Figure 4 [6, 18–20]. The porosity is then determined by using the following equation:

$$n = \frac{(M - M_d)}{V_s} \times 100, \tag{2}$$

where M is the mass of the wet specimen after an imbibition time t, M_d is the mass of the dry specimen, and V_S is the volume of the specimen.

3. Experimental Benchmark

The schematic diagram of the entire device is shown in Figure 5, where the purpose is to monitor the moisture front (wetting and saturation front, moisture gradient) and to assess the kinetics of the moisture gradient. This device includes a water storage tank (1) that ensures the water supply source, a supply line (2) that leads water to the water container, a discharge line (3), connected to a pump, that ensures the evacuation of excess water, a masonry wall (4), a computer (5), for data processing and the plotting of curves, a moisture sensor (6), for measuring of moistures rates, a water container (7), as an imbibition tank, a steel mesh support (8), to support the wall while letting the water pass, a baseplate (9) and a water tank support (11) as a support for the water container, thus blocking its deformations, a wall stabilization support (10). Other materials consist of a graduated ruler for measuring the heights of the wetting and saturation fronts, a stopwatch for recording time and time intervals between measurements, and a camera to capture the moisture gradient mapping on the walls.

4. Experimental Method

The method used is an experimental simulation in the laboratory, allowing us to multiply the wall models from variations of porosity. The phenomenon studied is assumed to be instantaneous, and the wall is assumed to be homogeneous. The moisture migration is vertical upwards, along the (o, z) axis. In the (o, x, y) plane, the moisture flow is uniform. The experiment is performed at temperature $(T \approx 29 \pm 5\,C)$ and ambient humidity $(RH \approx 81 \pm 2\%)$ controlled.

The device works as follows: masonry wall (4) of given lengths $(40 \sim 82\,cm)$, thickness $(15 \sim 20\,cm)$, and height $(64\,cm)$ is carried out suitably, using cement mortar bricks, and joints of $2\,cm$ thickness. Once carried out, the wall is then left for two (02) weeks for complete drying. To punctually follow the moisture profile on both sides, the wall is meshed using a cordex respecting a spatial step of 5 cm along the length and 3 cm across the thickness (see elements (12) and (13) in Figure 5). Moisture front heights are then measured using a transparent ruler suitably graduated to the nearest millimeter. Height measurements are made at each mesh point along the length from $y = 0\,cm$ to $y = 40 \sim 82\,cm$ with a step of $5\,cm$ and along the thickness from $x = 0\,cm$ to $x = 15$ to $20\,cm$ with a space step of $3\,cm$ (see Figure 6). The measurements are taken at a variable time interval between 1 and 24 hours. The moisture rates are measured at a variable time interval between $1 \sim 24$ hours, using the humidity sensor (6).

To follow the moisture rate in the masonry wall, the points are materialized at a height of 3 cm from the base of the wall, where the moisture sensors will be fixed punctually in order to have a specific moisture rate value, and at regular intervals of times. The percentage values of the moisture rates are routed to the computer (5) via a data acquisition system (Figure 5(a)). The results of the experiment can be expressed in the form of characteristic coefficients of the wetting kinetics (k_w) and the kinetics of saturation (k_s), or in graphical form. The characteristic coefficient of saturation

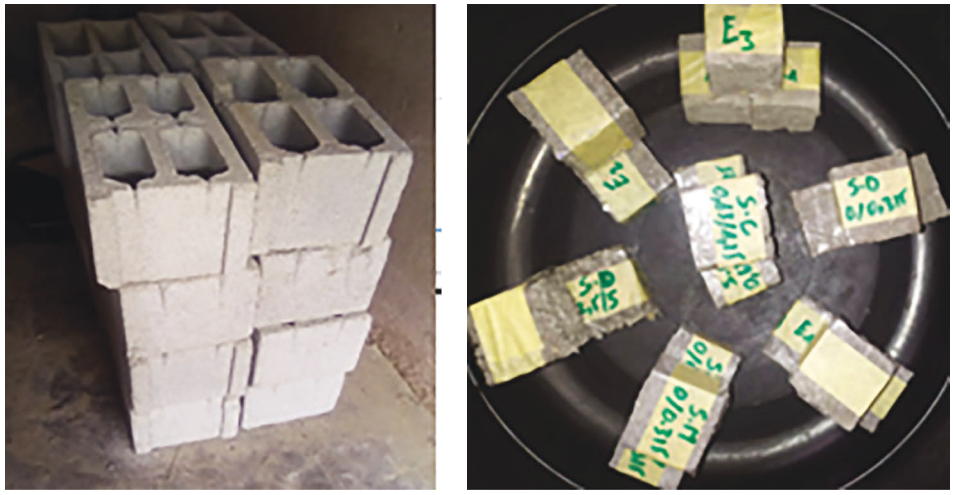

(a) (b)

Figure 3: (a) 20x20x40 cm breeze blocks and (b) cubic mortar blocks.

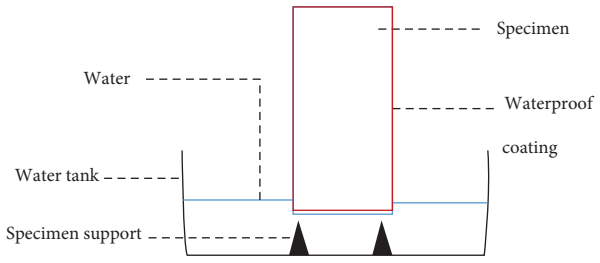

Figure 4: Principle diagram for measuring percolating porosity.

kinetic is the slope of the curve of saturation, given by Equation (1), and the characteristic coefficient of the wetting kinetic is the slope of the curve of wetting, given by Equation (2).

$$k_s = \frac{(m_{\text{saturation}} - m_{\text{initial}})}{t_{\text{saturation}} - t_{\text{initial}}},$$
$$k_w = \frac{(m_{\text{wetting}} - m_{\text{initial}})}{(t_{\text{wetting}} - t_{\text{initial}})}, \quad (3)$$

where $m_{\text{saturation}}$ is the moisture rate at saturation measured at the corresponding time $t_{\text{saturation}}$, m_{wetting} is the wetting moisture rate measured at the corresponding time t_{wetting}, and m_{initial} is the initial moisture rate, before wetting measured at the corresponding initial time t_{initial}. The graphical results give the spatial and temporal evolution of the wetting font through the wall, the spatial and temporal evolution of the saturation front, and the spatial and temporal evolution of the moisture rate time t_n,

5. Results and Discussion

5.1. Raw Material Characteristics. The results of the particle size analysis of the LQS and MQS as shown in Figure 7 show that globally all the grain sizes are in the fraction between 0.16*mm* and 5*mm*. The weight distribution of these sizes is well balanced in the sand samples. Furthermore, Hazen's uniformity coefficients lead to 4.09 and 3.50 for the MQS and LQS, respectively, meaning a varied or spread-out grain size. Furthermore, according to the analysis, the curvature coefficients of different sand samples are higher than 1, proving its good grading (presence of a large variety of grain sizes). Calculations of the fineness modulus of the samples give 3.15 for the MQS, indicating a low presence of fine elements in this sample. In contrast, a fineness modulus equal to 2.45 for the LQS indicates a high presence of fine elements in this sample.

For the preparation of mortars based on sand divided into granular classes, the determination of the granular classes was based on the NF P 18 – 101 standard. Thus, we have identified three granular classes, for the SCL sample as shown in Figure 7. The granular classes considered are 0.16/0.315 *mm*, 0.63/1.25 *mm*, and 2.5/5*mm*.

The results of the apparent densities of the LQS and MQS are reported in Table 2. The unfractionated MQS is denser than the fractionated LQS samples. The density of the LQS increases when the granular class contains smaller grain sizes.

5.2. Porosity Rate of Breeze Blocks. Let's call VBBW the vibrated breeze block wall, OBBW the ordinary breeze block wall, and $W1$ the wall whose breeze blocks are made of granular class 0.16/0.315 *mm*, $W2$ the wall whose breeze blocks are made of granular class 0.63/1.25 *mm*, and $W3$ the wall whose breeze blocks are made of granular class 2.5/5*mm*. The results of the percolating porosities of the specimens are shown in the histogram in Figure 8. The porosity rate decreases when the specimen is compacted. Indeed, the compaction of the breeze blocks leads to a drop in the porosity rate of around 13.04%. In addition, the extreme granular classes have higher porosity rates. Thus, the porosity rate increases by 10.48% from $W2$ to $W3$ and by 4.11% from $W1$ to $W3$.

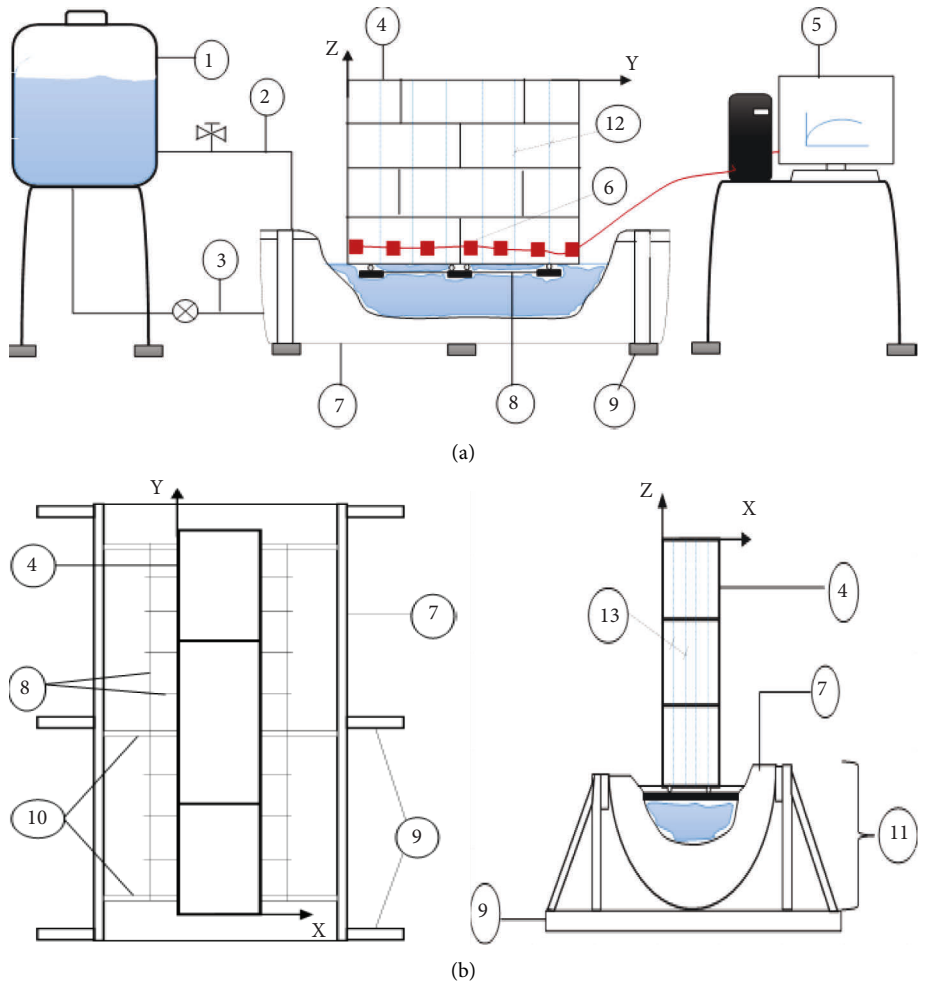

Figure 5: Schematic diagram of the experimental simulation benchmark of capillary water migration in the walls. (a) Elevation view along the length of the wall, (b) Top view, (c) Elevation view along the thickness of the wall, in which: (1) Water storage tank, (2) Supply line, (3) Discharge line, (4) Masonry wall, (5) Computer, (6) Humidity sensor, (7) Water container, (8) Steel mesh support, (9) Baseplate, (10) Wall stabilization support, (11) Water tank support, (12) Longitudinal meshing, (13) Transversal meshing.

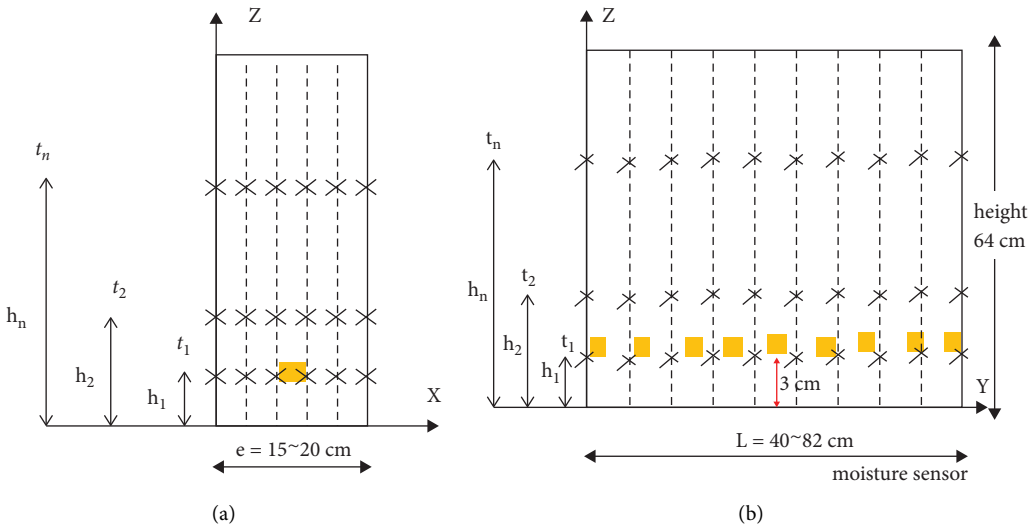

Figure 6: Schematic diagram of the principle of monitoring the capillary migration of the moisture front and rate in the walls; (a) On the thickness (o, x), (b) On the length (o, y). e thickness, L length, h_n humidity front at a given time t_n, m_n humidity front at a given time t_n.

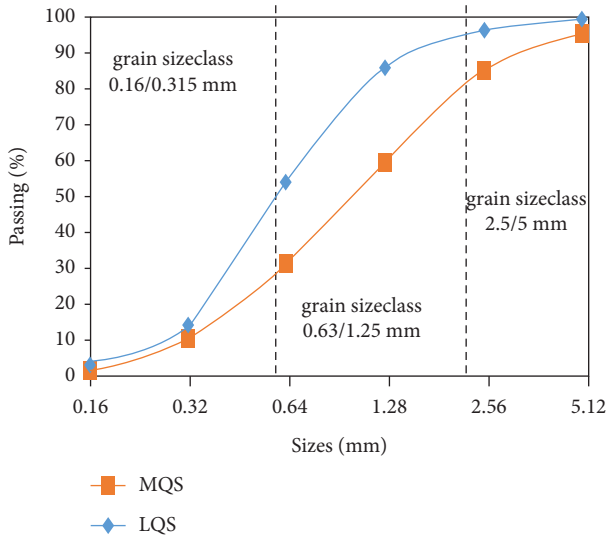

Figure 7: Graph of the particle size distribution of the sand samples.

Table 2: Results of apparent densities of the sand samples.

Samples	Granular classes (mm)	Density (g/cm^3)
LQS	0/0.315	1.479
	0.63/1.25	1.410
	2.5/5	1.359
MQS	0/5	1.582

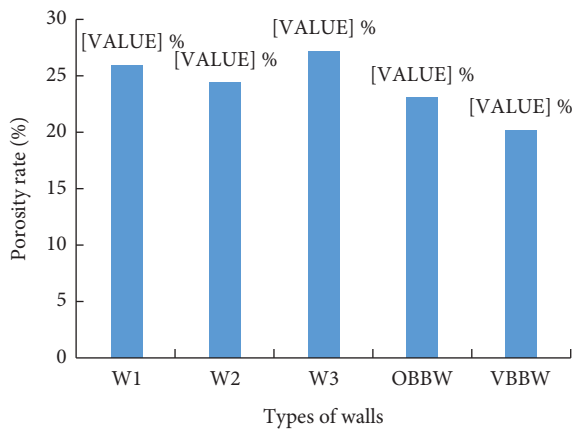

Figure 8: Porosity rate of mortar specimens.

6. Presentation of the Results of the Experiment

6.1. Influence of the Compactness of Breeze Blocks on the Dynamics of Moisture Migration

6.1.1. Spatial Distribution of Moisture Rate. Figure 9 shows the moisture rate according to the thickness of the masonry, after 48 hours of imbibition of VBBW (dashed lines) and OBBW (solid lines). The distribution of the moisture gradient through the thickness shows a significant phase shift in the absorption kinetics of the two walls. Indeed, the capillary saturation velocity is higher in the case of VBBW than in OBBW.

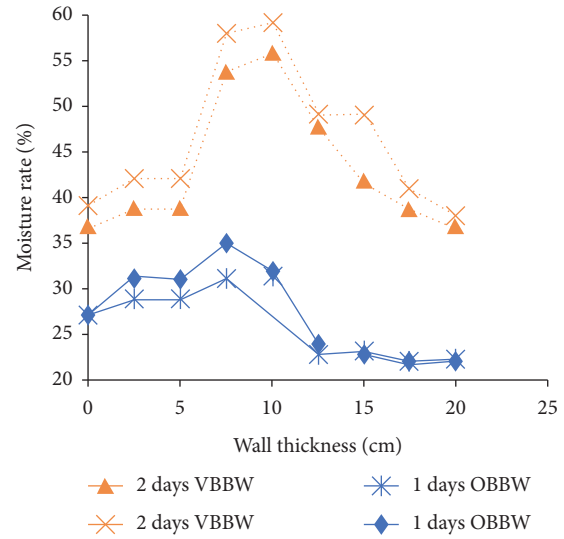

Figure 9: Curves of spatial distribution of moisture rates in walls.

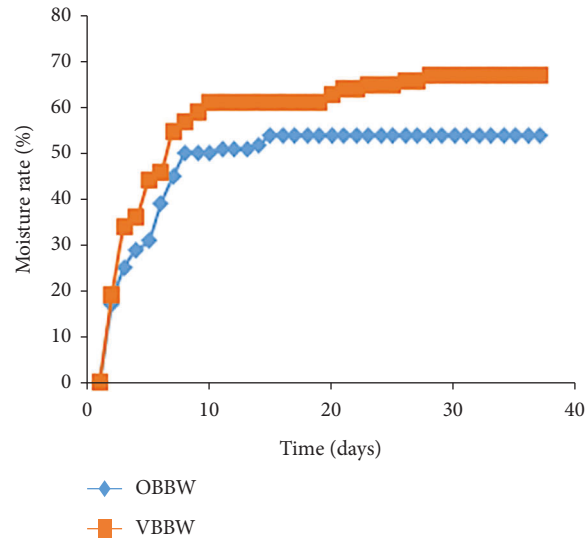

Figure 10: Curve of temporal evolution of moisture rates in walls.

6.1.2. Temporal Evolution of the Moisture Rate. Figure 10 shows the temporal evolution of the moisture rate of VBBW and OBBW, imbibed continuously for over 40 days. The curves have the same increasing paces and then evolve in an approximately horizontal step, characterizing a state of water saturation of the material. However, the absorption kinetics leading to this saturation state is greater for VBBW than for OBBW. Indeed, during the first phases of imbibition, wetting of the capillary walls occurs (monomolecular absorption), which requires less time to cover the small pore surface that characterizes the VBBW microstructure compared to the large pore surface that characterizes the OBBW microstructure.

Table 3: Characteristic values of wall moisture.

Wall types	Saturation speed	Saturation rate	Comparative values
VBBW	$k_s(V) = 7.375\%/\text{day}$	$HR_{sat}(V) = 66.75\%$	$k_s(O)/k_s(V) = 0.85$
OBBW	$k_s(O) = 6.25\%/\text{day}$	$HR_{sat}(O) = 54\%$	$HR_{sat}(O)/HR_{sat}(V) = 0.764$

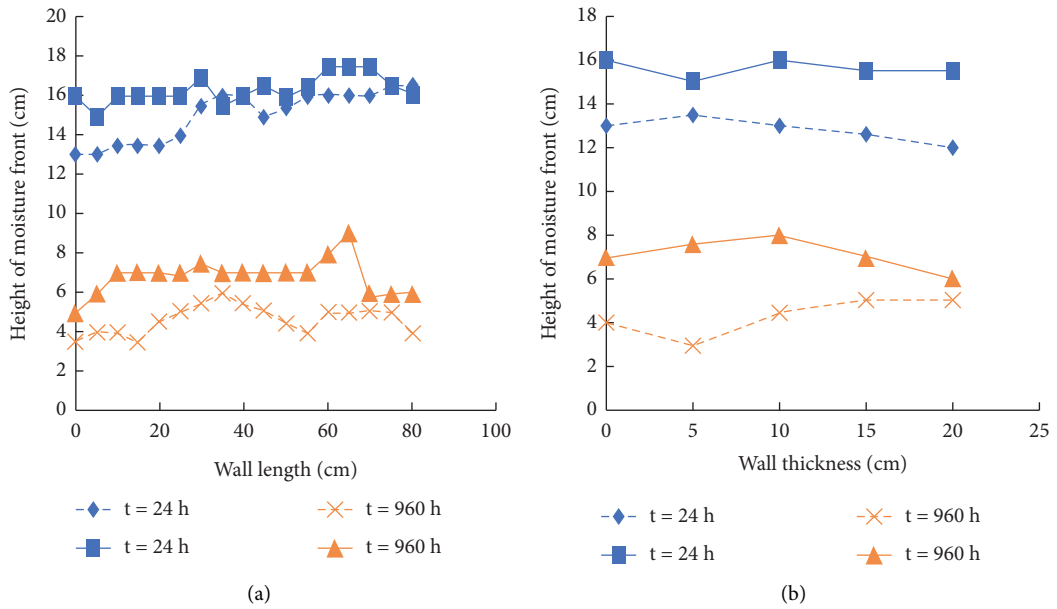

Figure 11: Evolution of the moisture fronts of the VBBW (solid lines) and the OBBW (dashed lines).

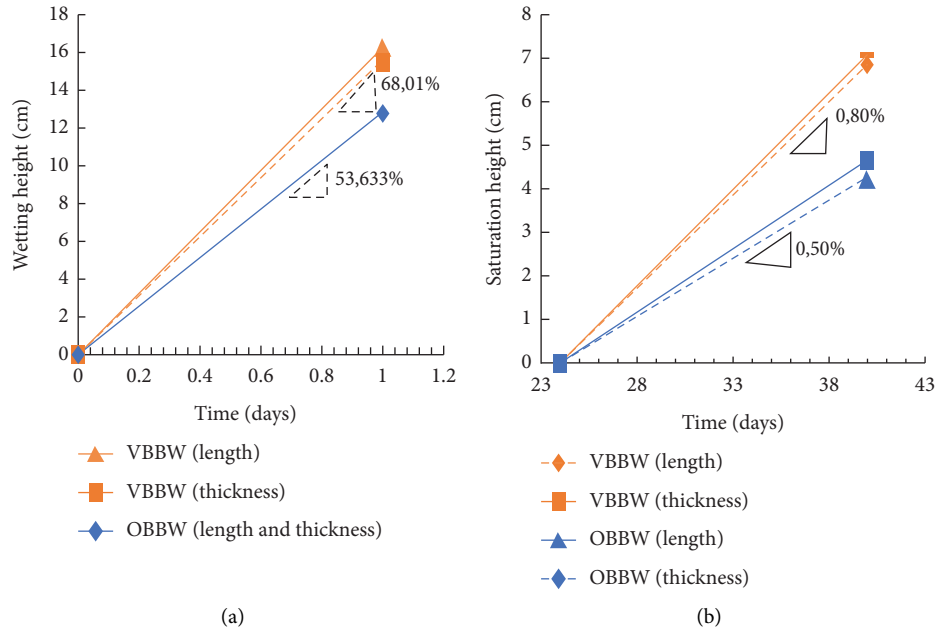

Figure 12: Moisture migration flow in VBBW and OBBW: (a) Wetting rate, (b) Saturation rate.

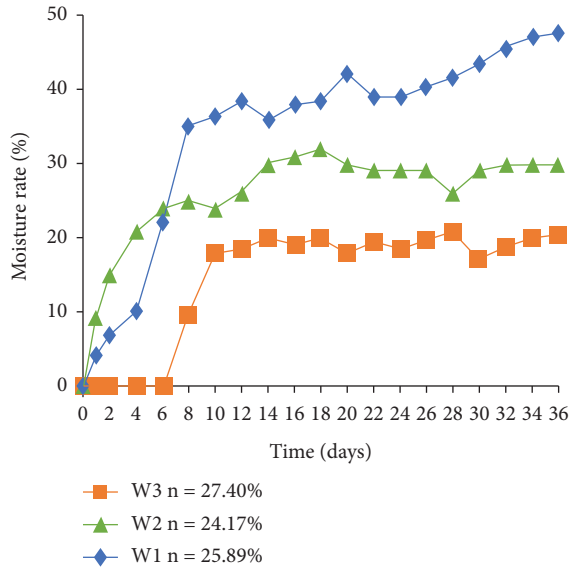

Figure 13: Temporal evolution of moisture rate.

Table 4: Characteristic values of moisture fluxes and rates at pseudo-saturation.

Granular classes (*mm*)	*M*3 2.5/5	*M*2 0.63/1.25	*M*1 0/0.315
Max flow before saturation	1.80%/day	2.60%/day	3.65%/day
Moisture rate at saturation	20.75%	30.50%	47.50%

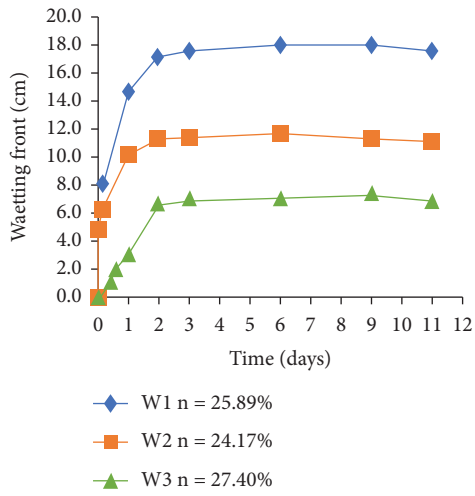

Figure 14: Temporal evolution of the wetting front.

Table 5: Characteristic values of wetting kinetics and maximum wetting front heights for the different walls.

Granular classes (*mm*)	*M*3 2.5 – 5	*M*2 0.63 – 1.25	*M*1 0 – 0.315
Migration flow of the wetting front	3.38 *cm*/day	5.65 *cm*/day	8.62 *cm*/day
Maximum height of the wetting front	7.42 *cm*	11.73 *cm*	18.18 *cm*

In addition, saturation is quickly reached for OBBW. Indeed, after 15 days, saturation is reached in this wall, against 28 days for the VBBW. Indeed, during the capillary absorption process leading to the saturation of the capillary channels, once the wetting of the capillary cavities has taken place, the migration of moisture leading to the establishment of a continuous water film is faster and more accentuated in the smaller capillary channels distributed in the solid phase of the VBBW.

It should also be noted that despite the high porosity of OBBW, the saturation moisture rate of this wall is lower than that of VBBW. Indeed, the saturation moisture rate in OBBW is 54%, compared to 67% in VBBW. This is due to a resistance to moisture migration, caused by the coarser capillaries distributed in the OBBW, thus slowing down the migration of moisture. As illustrated by the characteristic values in Table 3, the low porosity rate of VBBW, as well as the high proportion of occluded pores and non-interconnected open pores formed during the vibration of these blocks during the manufacturing process, can give the wall a resistant character to moisture migration. However, this will be in contrast to the high proportion of smaller pore sizes and therefore favourable to high capillary absorption of moisture.

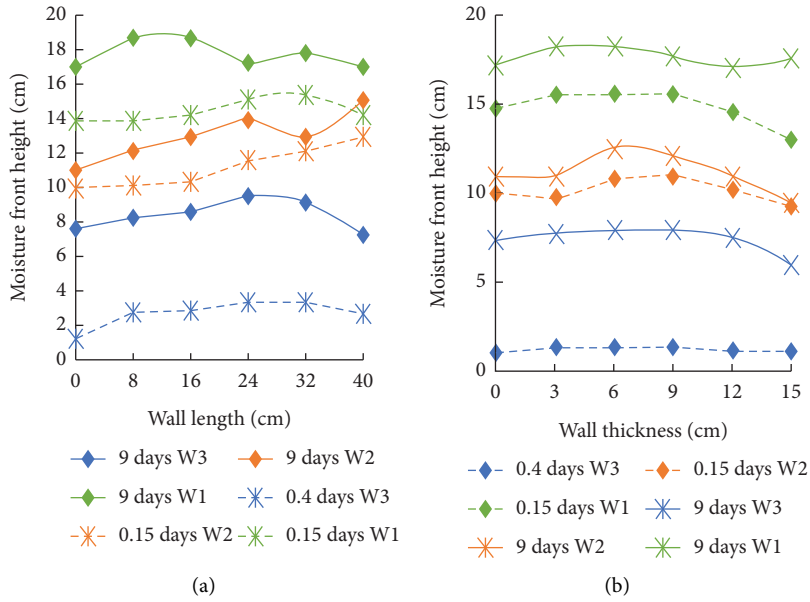

Figure 15: Comparison of the spatial temporal evolution of moisture fronts.

6.1.3. Spatial Evolution of the Moisture Front. The evolution of the moisture fronts (wetting and saturation) of the VBBW (solid lines) and the OBBW (dashed lines) is illustrated in (Figure 11). Moisture profiles are plotted along length (Figure 11(a)) and along thickness (Figure 11(b)). A higher saturation front appears for VBBW, compared to OBBW where the front level remains lower. The migration flows of the wetting and saturation fronts presented in Figures 12(a) and 12(b) corroborate this result. The dephasing between the two walls is justified by the reduction in pore size caused by the vibration of the blocks during their manufacture. The first immediate consequence is the prolonged time it will take for the liquid to migrate from one level of the wall to another; the second consequence is the slowness saturation of the pore network, as presented by the result in Figure 9. The resistance to moisture migration in OBBW is explained by the presence of a large proportion of large pores, which do not participate significantly in the dynamics of capillary moisture migration.

6.2. Influence of Granular Classes of Mortar Sand

6.2.1. Temporal Evolution of the Moisture Rate. Figure 13 shows the temporal evolution of the moisture rate of these walls after continuous imbibition for more than 36 days. On analysis, the flow curves, independently of the granular class, are globally well represented, and qualitatively in agreement with the works shown in [11, 14].

The starting of the imbibition process shows a gap according to the granular class; thus, the wall M3 starts its saturation 6 days after the walls M1 and M2. After starting up, the curves have the same increasing paces and then evolve in an approximately horizontal step, characterizing a state of pseudosaturation. However, the absorption kinetics leading to this pseudosaturation state varies from one granular class to another as indicated by the characteristic values in Table 4. These observations show the influence of the grain sizes of the granular class on the dynamics of moisture migration in walls. Migration kinetics and moisture rate at saturation decrease as the grain sizes of the granular class increase, which is in agreement with results found in [21].

Furthermore, the addition of aggregates to the cementatious matrix considerably modifies its porous microstructure, in the sense of increasing its tortuosity. The presence of the sand aggregate in the cementatious matrix acts as a barrier to gel and capillary pores, and although the ITZ is a moisture migration path, its highly sinuous nature increases with grain size, thus providing a resistant character to moisture migration.

The high moisture absorption rate of $M1$ could be explained by the high content of fine particles in this fraction. Indeed, the large amount of fines in the mortar absorbs a larger part of the mixing water, with the consequence of limiting the hydration process of the cement, which should however contribute to the modification of the capillary porosity in the sense of reducing the sizes of the capillary pores, and making them discontinuous.

6.2.2. Temporal Evolution of the Wetting Front. Figure 14 shows the temporal evolution of the wetting fonts of walls $M1, M2$, and $M3$. The capillary rise curves show that surface wetting occurs on average within an interval of 2 days during which the kinetics of the process vary from one granular class to another. It is important to note that the wetting height reached at this time also varies from one

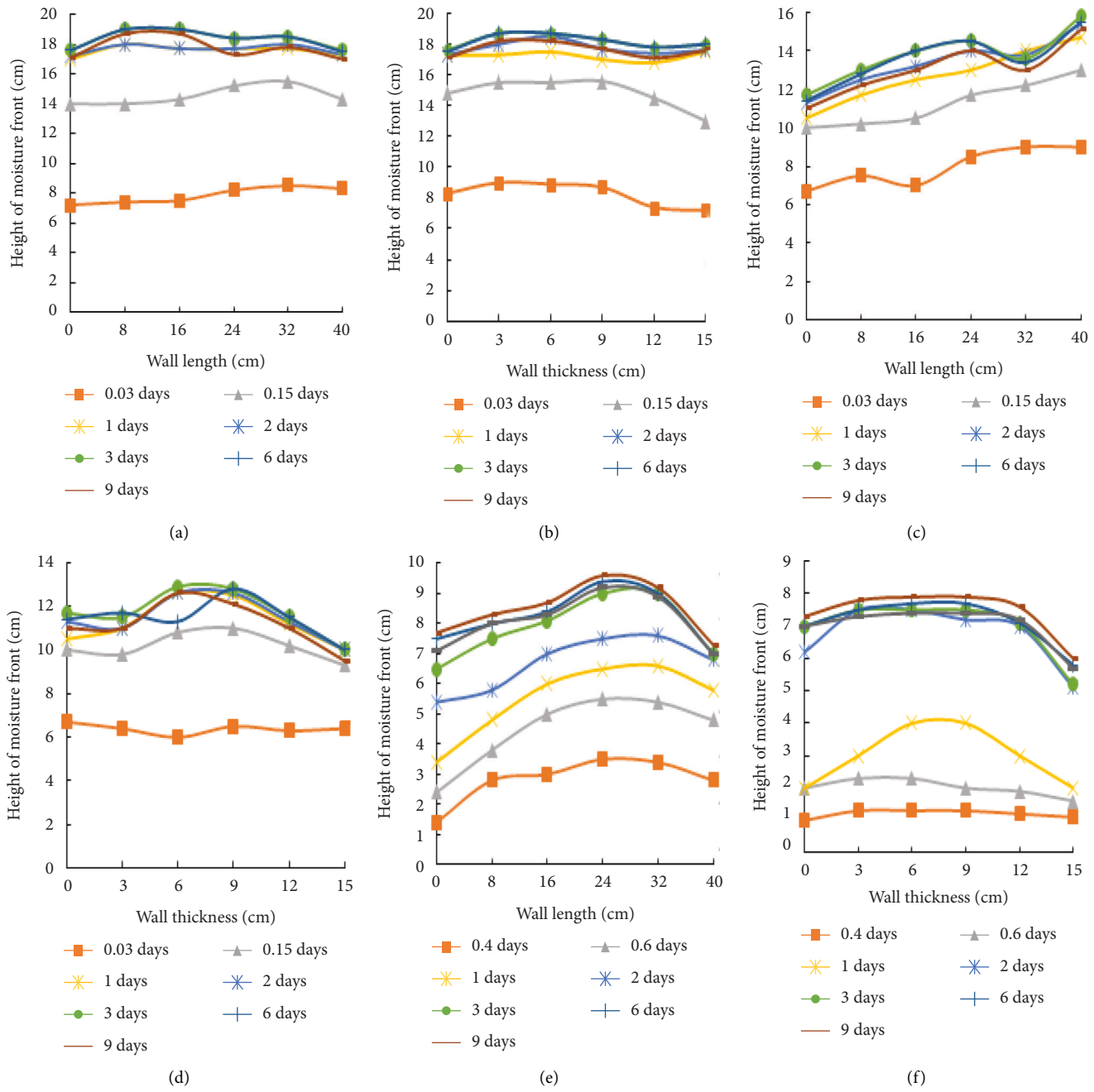

Figure 16: Spatial and temporal evolution of wall moisture front profiles: ((a)-(b)) M1, ((c)-(d)) M2 and ((e)-(f)) M3.

granular class to another and independently of these classes, and the level value of the front remains constant for the next 9 days, before gradually disappearing leaving discontinuous moisture gradients on the walls. As summarized by the characteristic values in Table 5, the wetting kinetics are slower for walls with large particle size granular classes, so are the step moisture fronts. In other words, the use of large particles in the manufacture of breeze blocks makes the wall resistant to rising damp.

6.2.3. Spatial and Temporal Evolution of the Wetting Front. The temporal-spatial evolution of the moisture fronts of the walls is shown in Figures 15(a) and 15(b) for wall M1,

Figures 15(c) and 15(d) for M2, and Figures 15(e) and 15(f) for wall M3. The dynamics of moisture migration are more important in breeze block walls containing sand of low granular classes ($M1$: 0.16/0.315 mm and $M2$: 0.63/1.25 mm). In contrast, the wall M3 with the largest granular class of sand (2.5/5mm) has a higher resistance to moisture migration as shown in Figures 16(a) and 16(b).

7. Conclusion

The realization of a device used to study the dynamics of moisture migration in masonry wall was the subject developed throughout this study and contributed to highlight the effects of compactness and granular class constituting the breeze block. Then, it appears that the normalized vibration of concrete blocks leads to a drop in the porosity rate, the disconnection of interconnected open pores, and the establishment of occluded pores. These modifications grant the wall resistance to moisture migration, but the impact of which is reduced by the pore sizes will be considerably reduced during the vibration process and therefore leads to increase in the migration dynamic. Large aggregates allow to obtain porous concrete blocks, with large pore sizes, resistant to capillary rising damp. This simple device is also a way to assess the rate of influence of W/C ratio, cement dosage, and cement hydration degree of breeze blocks, on moisture dynamic in the wall; this would be possible with a larger database. We also want to see this device improved through the addition of a quantified pressure variation accessory, with automation of some controls making the device more convenient and reliable.

Data Availability

No data were used to support this study.

Conflicts of Interest

The authors declare that they have no conflicts of interest.

References

[1] R. D. Pasquantonio, G. A. Parsekian, F. S. Fonseca, and N. Gshrive, "Experimental and numerical characterization of the interface between concrete masonry block and mortar," *Revista IBRACON de Estruturas e Materiais*, vol. 13, no. 3, pp. 578–592, 2020.

[2] Z. Lafhaj, M. Goueygou, A. Djerbi, and M. Kaczmarek, "Correlation between porosity, permeability and ultrasonic parameters of mortar with variable water/cement ratio and water content," *Cement and Concrete Research*, vol. 36, no. 4, pp. 625–633, 2006.

[3] S. Diamond and J. Huang, "The ITZ in concrete- A different view based on image analysis and SEM observations," *Cement and Concrete Composites*, vol. 23, no. 2-3, pp. 179–188, 2001.

[4] D. N. Winslow, M. D. Cohen, D. P. Bentz, K. A. Snyder, and E. J. Garboczi, "Percolation and pore structure in mortars and concrete," *Cement and Concrete Research*, vol. 24, no. 1, pp. 25–37, 1994.

[5] M. K. Head and N. R. Buenfeld, "Measurement of aggregate interfacial porosity in complex, multi-phase aggregate concrete: binary mask production using backscattered electron, and energy dispersive X-ray images," *Cement and Concrete Research*, vol. 36, no. 2, pp. 337–345, 2006.

[6] S. P. Zhang and L. Zong, "Evaluation of relationship between water absorption and durability of concrete materials," *Advances in Materials Science and Engineering*, vol. 2014, Article ID 650373, 2014.

[7] E. Franzoni, "Rising damp removal from historical masonries: a still open challenge," *Construction and Building Materials*, vol. 54, pp. 123–136, 2014.

[8] E. Franzoni, "State-of-the-art on methods for reducing rising damp in masonry," *Journal of Cultural Heritage*, vol. 31, pp. S3–S9, 2018.

[9] F. Sandrolini and E. Franzoni, "An operative protocol for reliable measurements of moisture in porous materials of ancient buildings," *Building and Environment*, vol. 41, no. 10, pp. 1372–1380, 2006.

[10] C. S. Tsakeu, E. Simo, J. I. C. Zambe, S. F. W. Tabekoueng, and S. N. Sob, "Building Heating Process: numerical analysis of the impact of moisture and the type of concrete," *Civil engineering and architecture*, vol. 9, no. 6, pp. 1785–1797, 2021.

[11] Z. Suchorab, D. Barnat-Hunek, P. Smarzewski, Z. Pavlík, and R. Černý, "Free of volatile organic compounds protection against moisture in building materials," *Ecological Chemistry and Engineering*, vol. 21, pp. 401–411, 2014.

[12] T. Chaussadent, V. Baroghel-Bouny, N. Rafaï, A. Ammouche, and H. Hornain, "Influence du rapport sur l'hydratation, la microstructure et les déformations endogènes de pâtes de ciment durcies," *Revue Franaise de Génie Civil*, vol. 5, pp. 217–230, 2001.

[13] J. Skramlik, M. Novotny, and K. Suhajda, *Determining moisture parameters in building materials*, Pan American Conference for NDT, Cancun, Mexico, 2011.

[14] I. Lukic, V. Radonjanin, M. Malešev, and V. Bulatovic, "Influence of mineral Admixtures on Water Absorption of Lightweight Aggregate concrete," in *Proceedings of the iNDiS 2015 - PLANNING, DESIGN, CONSTRUCTION AND RENEWAL IN THE CIVIL ENGINEERING*, pp. 25–27, Novi Sad, Serbia, November 2015.

[15] B. Larbi, W. Dridi, P. Le Bescop, P. Dangla, and L. Petit, "Link between microstructure and tritiated water diffusivity in mortars," *EPJ Web of Conferences*, vol. 56, Article ID 01006, 2013.

[16] E. Simo, P. D. Dzali Mbeumo, and J. C. Mbami Njeuten, "Moisture transfer in concrete: numerical determination of the capillary conductivity coefficient," *Slovak Journal of Civil Engineering*, vol. 25, no. 1, pp. 10–18, 2017.

[17] N. M Nde, D. Fokwa, M. Mbessa, T. T Tamo, and C. Pettang, "Numerical simulation of the influence of pores sizes on moisture migration dynamic in masonry wall," *International Journal of Engineering & Technology*, vol. 10, no. 2, pp. 164–169, 2021.

[18] N. Chousidis, E. Rakanta, I. Ioannou, and G. Batis, "Influence of iron mill scale additive on the physico-mechanical properties and chloride penetration resistance of concrete," *Advances in Cement Research*, vol. 28, no. 6, pp. 389–402, 2016.

[19] Y. Wang, L. Li, M. An, Y. Sun, Z. Yu, and H. Huang, "Factors influencing the capillary water absorption characteristics of

concrete and their relationship to pore structure," *Applied Sciences*, vol. 12, no. 4, p. 2211, 2022.

[20] T. Meng, H. Wei, K. Ying, M. Wang, and M. Wang, "Analysis of the effect of nano-SiO2 and waterproofing agent on the water transportation process in mortar using NMR," *Applied Sciences*, vol. 10, no. 21, p. 7867, 2020.

[21] H. T. Ghashghaei and A. Hassani, "Investigating the relationship between porosity and permeability coefficient for pervious concrete pavement by statistical modelling," *Materials Sciences and Applications*, vol. 7, no. 2, pp. 101–107, 2016.